THE ASTROPHYSICAL JOURNAL, 463:L55–L58, 1996 June 1

NEAR-INFRARED IMAGING SPECTROSCOPY OF IRAS FSC 10214+4724: EVIDENCE FOR A STARBURST REGION AROUND AN ACTIVE GALACTIC NUCLEUS AT $z = 2.3$

H. KROKER, R. GENZEL, A. KRABBE, L. E. TACCONI-GARMAN, M. TECZA, AND N. THATTE
Max-Planck-Institut für extraterrestrische Physik (MPE), Postfach 1603, D-85740 Garching bei München, Germany

AND

S. V. W. BECKWITH
Max-Planck-Institut für Astronomie (MPIA), Königstuhl 17, D-69117 Heidelberg, Germany
Received 1995 December 18; accepted 1996 March 6

ABSTRACT

We report 1″ imaging spectroscopy of the 1.95–2.4 μm wavelength region in the $z = 2.284$ galaxy IRAS FSC 10214+4724. We find that the rest-frame Hα and [N II] emission have different spatial extents. We also detect broad ($\Delta v_{\rm FWZP} \approx 3500$ km s^{-1}) Hα emission. FSC 10214 is a very luminous gravitationally lensed galaxy, which intrinsically contains both a type 1 active galactic nucleus and a more extended star-forming disk. The AGN and circumnuclear star formation both contribute significantly to the total luminosity of $\sim 10^{13}\ L_\odot$.

Subject headings: galaxies: active — galaxies: individual (FSC 10214+4724) — infrared: galaxies

1. INTRODUCTION

Based on its far-infrared spectrum and submillimeter-CO emission, the $z = 2.284$ *IRAS* source FSC 10214+4724 (hereafter F10214) has been interpreted to be a hyperluminous galaxy in an early superstarburst ($\geq 10^{14}\ L_\odot$ for $H_0 = 75$ km s^{-1} Mpc^{-1}, $q_0 = 0.5$, 1″.0 = 5.3 kpc; Downes, Solomon, & Radford 1995; Rowan-Robinson et al. 1991, 1993; Scoville et al. 1995). However, recent *Hubble Space Telescope* (Eisenhardt et al. 1996) and ground-based imaging of the rest-frame UV (Broadhurst & Lehár 1995) and visible emission (Graham & Liu 1995) now strongly suggest magnifications by factors between 5 and 100 due to a foreground gravitational lens. The rest-frame UV/visible emission lines and the UV polarization resemble those of Seyfert II nuclei (Elston et al. 1994; Lawrence et al. 1993; Soifer et al. 1995; Iwamuro et al. 1995). In this Letter, we present 1″ near-infrared imaging spectroscopy indicating that F10214 is a composite object, with an active galactic nucleus (AGN) and circumnuclear star formation both contributing to the total luminosity.

2. OBSERVATION AND DATA REDUCTION

We observed F10214 in the K band (1.95–2.4 μm) with the new MPE imaging spectrometer, 3D, in 1995 January at the 3.5 m telescope on Calar Alto, Spain. Detailed descriptions of the 3D instrument and the data reduction are given in Weitzel (1994), Weitzel et al. (1996), Krabbe et al. (1995), and Genzel et al. (1995). Briefly, for a 16×16 pixel field of sky, 3D obtains 256 channel spectra of the entire K band simultaneously for each 0″.5 pixel. This is achieved by optically rearranging the spatial field into a long slit using two mirror sets, followed by a cooled grating spectrometer with spectral resolving power of $R = 1100$ (FWHM, sampled at $R_N = 2200$) on a 256^2 NICMOS 3 detector. The seeing during the observations was 1″ FWHM at 2 μm. For sky subtraction, we alternated on-source exposures (200 s) with observations of blank sky 30″ away from the source. The total on-source integration time was 18,000 s, of which we selected the best 9000 s. The data reduction with the GIPSY package (van der Hulst et al. 1992) includes background subtraction, flat-fielding, correction for bad pixels and cosmic-ray hits, spectral calibration (neon lamp) and rebinning onto a linear wavelength grid of 2 nm step size, rearranging onto a $16 \times 16 \times 300$ pixel data cube, rebinning onto a 0″.25 spatial grid, co-adding and centering of the individual exposures on the Hα + [N II] peak, dividing by a normalized F8 star spectrum, and spatially smoothing to the original resolution. Fluxes and flux densities are based on the K-band magnitudes of Lawrence et al. (1993).

3. RESULTS

3.1. *Spectral Characteristics*

Figure 1 (*top*) shows K-band spectra (2″.25 aperture) of the Hα peak of F10214, as well as 4″ southwest of it. The noise level increases toward longer wavelengths because of the rapid rise in thermal background. In addition to the strong lines Hα + [N II] $\lambda\lambda$6548, 6583, [O I] λ6300, and [S II] $\lambda\lambda$6716, 6731 may be present at the 3–4 σ level, consistent with the $R = 80$ spectroscopy of Soifer et al. (1995). From Hα + [N II] $\lambda\lambda$6548, 6583, we derive a redshift $z = 2.284 \pm 0.001$, in agreement with Elston et al. (1994). The rest-frame visible lines thus appear to be 180 km s^{-1} blueshifted relative to the centroid of the CO ($3 \rightarrow 2$) emission ($z = 2.2854 \pm 0.0001$, Downes et al. 1995; $z = 2.2853 \pm 0.0003$, Scoville et al. 1995), although they lie just within our error bars. The overall rest-frame R-band spectrum of F10214 resembles an AGN, in agreement with Elston et al. (1994).

3.2. *Line and Continuum Maps: Differences in the Spatial Distribution*

Figure 2 (Plate 3) shows line and continuum maps obtained with 3D overlayed on the 0″.4 FWHM K-band image of Graham & Liu (1995; *gray scale*). Our key new findings are the different spatial morphologies in all of these maps: Hα and [N II] line emission is restricted to the immediate neighborhood of the brightest and southernmost continuum source of the F10214 complex (source 1 in the terminology of Matthews et al. 1994). No significant line emission is found in sources 2, 3, or 4, anywhere in the K band. The [N II] emission is fairly compact but is marginally extended in an east-west direction,

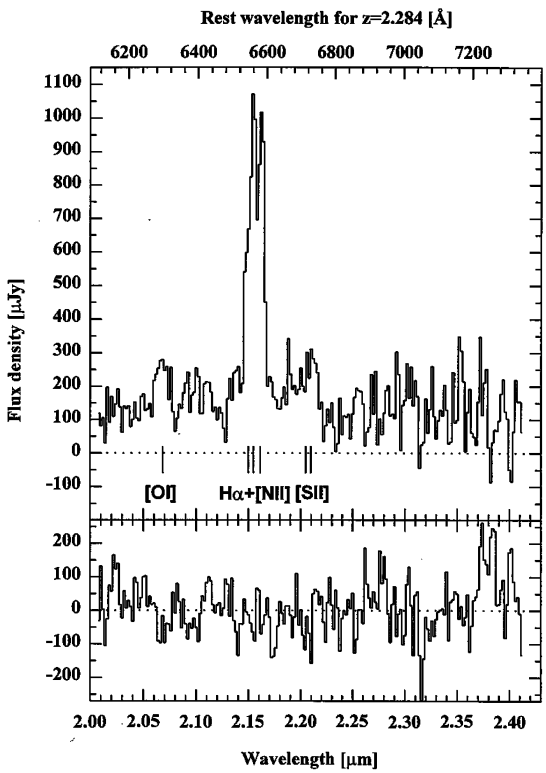

FIG. 1.—3D *K*-band spectra of a 2.″5 diameter aperture, centered on component 1 of F10214, binned in 2 nm channels. Positions of several lines for a redshift of $z = 2.284$ are marked. The lower spectrum corresponds to a region 4″ southwest of the source.

as concluded by Matthews et al. (1994). In contrast, Hα shows the same compact core, but is significantly more extended east-west in fainter emission, following approximately the 1.″5–2″ arc structure of source 1 (Graham & Liu 1995). Line-free *K* continuum is visible in source 1 as well, and has an extension north of it at the position of source 2 (Fig. 2, *right panel*). Source 2 is weaker than source 1 by a factor of 2. An integrated 1.95–2.4 μm map reconstructed from the 3D data cube (not shown) is in excellent agreement with the broadband Keck images of Matthews et al. (1994) and Graham & Liu (1995). Thus, we conclude that a significant fraction of the east-west extent in the *K*-band maps is due to line emission.

3.3. *Broad* Hα *Emission*

We have fitted multiple Gaussians to the Hα/[N II] $\lambda\lambda$6548, 6583 spectra for different spatial regions: aperture sizes of 0.″75, 1.″25, 1.″75, and 2.″25, centered on the Hα peak; two ringlike regions containing the flux from the 2.″25 aperture, but not the central 0.″75 and 1.″25 aperture, respectively; and, finally, a region covering just the wings (more than 0.″7 east-west distance from the center) of the 2″ arc (source 1). In a first step, we fitted three single Gaussians to the Hα and the two [N II] lines. The fit was constrained by fixing the relative positions of the [N II] and Hα lines and by forcing all three lines to have the same width and continuum level, resulting in a total of five free parameters for ~23 significant data points. This fit resulted in a [N II] λ6583/[N II] λ6548 line ratio of about 2:1, instead of 2.98:1, as required by their Einstein *A*-values and wavelengths. Fixing the [N II] line ratio to 2.98:1 results in a fit with unacceptably large residuals (Fig. 3*a*). Thus, a three-component model does not fit our data. In order to maintain a 2.98:1 [N II] λ6583/[N II] λ6548 flux ratio, it is necessary to add emission contributing significantly blueward of the Hα peak and especially accounting for the line wing to the blue of [N II] λ6548. The most plausible such component is a broad Hα emission line. A fit with a velocity-shifted fourth narrow line does not give convincing results. As demonstrated in Figures 3*b*–3*d*, the fits using a fourth, broad Gaussian centered on the narrow Hα line (resulting in a total of seven free parameters) are very satisfactory (the reduced χ^2 is near 1). The contribution of broad Hα to the total line flux of the Hα + [N II] line system is 50% for a 2.″25 aperture, the line width is 2400 km s^{-1} FWHM (FWZP = 3500 km s^{-1}) for all fitted regions, while the FWHM of the three narrow lines is 600 ± 100 km s^{-1}. Thus, we conclude that the nucleus of F10214 contains a buried broad-line region and, therefore, is likely to have a type 1 (Seyfert I or QSO) nucleus.

3.4. *Extended* Hα *Emission: Circumnuclear Star Formation*

The [N II] λ6583/Hα_{broad} line ratio does not vary with aperture size, which is consistent with a dominating compact AGN origin of both lines (Fig. 4). A shift in line velocities as a function of position could not be found. The contribution from the underlying galaxy to the [N II] emission is small, according to the limits given by the error bars in Figure 4. Therefore, we finally constrained the fit by fixing the [N II] λ6583/Hα_{broad} line ratio and fitted six parameters to our data set: a narrow and a broad line width, two amplitudes, a wavelength position, and a continuum level. In contrast, the [N II] λ6583/Hα_{narrow} line ratio shows spatial variation in our data; it drops from 1.66 ± 0.06(1 σ) in a peak-centered 0.″75 aperture to 1.2 ± 0.16 within a 2.″25 aperture (Fig. 4). In the extreme wings of the 2″ arc, the ratio is 0.6 ± 0.2. Thus, we find that 30% of the total narrow Hα flux is in an east-west extended component, corresponding to the 2″ arc in the Keck K_s-band image of Graham & Liu (1995). For small apertures, the [N II] λ6583/Hα_{narrow} line ratio is consistent with a classical photoionized narrow-line region. In contrast, in the east-west wings that undiluted ratio is $\leq$0.5 and resembles that of an H II region galaxy ([N II] λ6583/Hα ~ 0.2–0.5; Osterbrock 1989, p. 346). We propose that this extended component is a star-forming disk and may be associated with the zone of far-infrared continuum (Rowan-Robinson et al. 1993) and submillimeter CO emission (Scoville et al. 1995; Downes et al. 1995). The dilution of this region by the flux from the central AGN can be derived from the [N II] λ6583/Hα_{narrow} line ratios. If the total [N II] flux originated from the AGN, the corresponding narrow Hα flux would be 0.6/1.7 = 0.35 times the total Hα flux. But some of the [N II] flux originates in the starburst region itself, leading to an even smaller contribution (~15%) of Hα from the AGN. Unfortunately, the signal-to-noise ratio substantially decreases in the outer region. However, the main signature of the changing physical conditions is the change in the [N II]/Hα ratio, which is a robust result. The fourth component (broad Hα) is not critical at all for this conclusion; in fact, just fitting three components would make the result even clearer because the [N II] λ6583/Hα_{narrow} line ratio would drop even more dramatically in the outer regions.

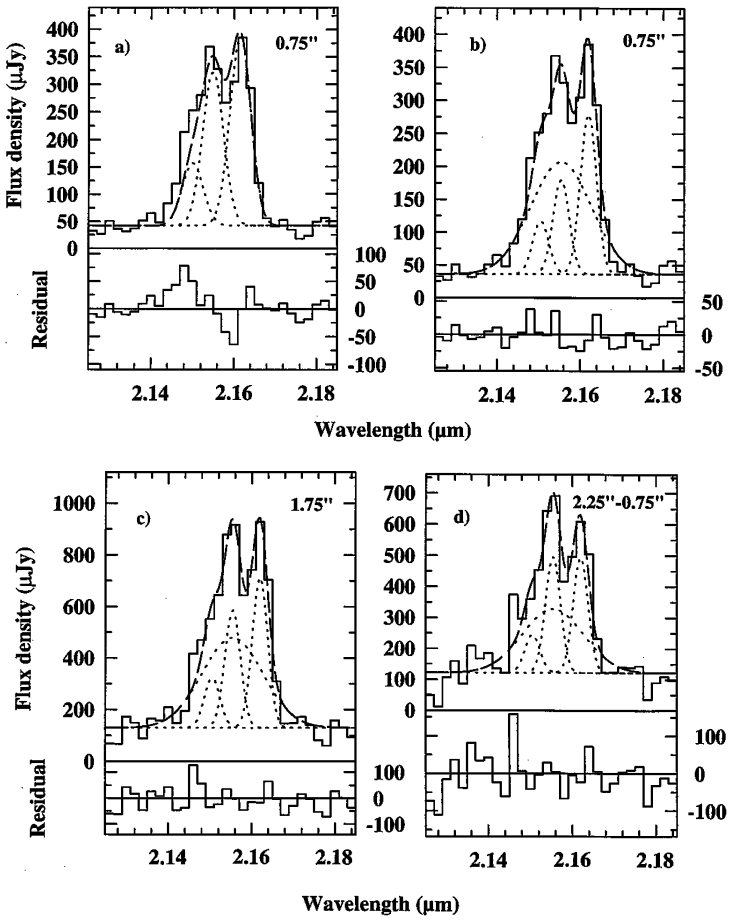

FIG. 3.—(*a*–*c*) Spectral line fits to the Hα + [N II] λλ6548, 6583 profile for three different apertures: (*a*) 0.″75 diameter, fitted by three Gaussians; (*b*) 0.″75 diameter, fitted by four Gaussians; (*c*) 1.″75 diameter, fitted by four Gaussians. (*d*) Annulus (2.″25–0.″75), fitted by four Gaussians. The histogram represents the data, the short-dashed lines are the four single-Gaussian fits, and the sum is drawn as a long-dashed line. Lower plots are the residuals of the fits.

3.5. *Energetics of F10214: Contributions of AGN and Star Formation*

From the observed broad- and narrow-line Hα fluxes, estimates of their extinctions, and model gravitational lens magnifications, it is now possible to derive a first rough estimate of the luminosities of these two components. The lens models of Broadhurst & Lehár (1995) and Eisenhardt et al. (1995) predict a magnification of 50–100 for the central (0.″7, intrinsic size ~0.″01 or 50 pc) bright component. For the more extended (2″, 0.″4, or 2 kpc intrinsic), fainter arc visible on the Keck-IR image (Graham & Liu 1995), the magnification is 5–10. This is probably also the size scale of the far-infrared continuum and CO (3 → 2) emission region (Downes et al. 1995; Scoville et al. 1995). In Table 1 we give an estimate of the BLR, NLR, and starburst contributions to the Hα flux. The visual extinction can be derived from the observed Hα/Hβ ratio. Since the AGN dominates the total flux, the observed Hα/Hβ ratio of 8.6 (Iwamuro et al. 1995) can be used for estimating the AGN extinction. For an intrinsic Hα/Hβ ratio of 3.1 in the NLR (Veilleux & Osterbrock 1987) and a foreground dust screen (probably applicable to BLR and NLR), this results in $A_V = 2.9$ and an extinction correction of

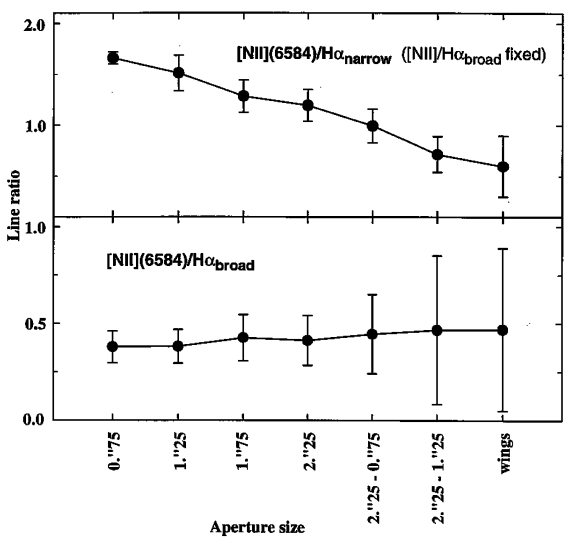

FIG. 4.—Line ratios for different aperture sizes (see text). Error bars are ±1 σ and are derived from the least-squares fits.

TABLE 1

DERIVED LUMINOSITIES OF VARIOUS COMPONENTS

Component	Observed Luminosity[a]	Extinction Correction	Magnification Factor	$L_{bol}/L_{H\alpha}$	L_{bol}
$H\alpha_{broad}$	16 ± 4	8	50–100	400–600[b]	500–1500
$H\alpha_{narrow}$	5 ± 1	8	50–100	180[b]	70–140
$H\alpha_{star\ formation}$	1.5 ± 0.5	10–100	5–10	200[c]	300–6000

[a] All luminosities are in $10^9\ L_\odot$.
[b] Netzer 1990.
[c] Case B recombination (e.g., Osterbrock 1989) and $L_{bol}/L_{Lyc} = 8$.

a factor of 8 according to a screen model [$I(H\alpha) = I_0 \exp(-\tau_{H\alpha})$, $\tau_{H\alpha} \approx 0.7A_V$]. For the circumnuclear region, obviously containing a large concentration of dense molecular gas and dust, a mixed dust-gas model is more likely, leading to much larger values for A_V. The CO fluxes of Scoville et al. (1995) and Downes et al. (1995) convert to $A_V \geq 10^2$ in the circumnuclear star-forming region if one adopts Galactic conversion factors from CO flux to H_2 column density and dust extinction. With $I(H\alpha) = I_0[1 - \exp(-\tau_{H\alpha})]/\tau_{H\alpha}$ (e.g., Thronson et al. 1990) and $\tau_{H\alpha} \approx 0.7A_V$, we therefore estimate that the extinction correction for the extended $H\alpha$ component is at least 10, and may even exceed 10^2. Finally, we can then convert the infrared intrinsic $H\alpha$ luminosities to bolometric luminosities by case B recombination theory for the star formation region, as well as by typical QSO NLR/BLR models for the AGN (Netzer 1990). The results are presented in Table 1. While the details are still quite uncertain, the basic result is clear. Both a powerful AGN and a very luminous circumnuclear star formation region contribute to the total luminosity of F10214. Thus, F10214 has intrinsically similar characteristics to those of other luminous *IRAS* galaxies (Condon et al. 1991; Genzel et al. 1995), although it is still one of the most luminous galaxies.

We are grateful to James R. Graham for providing us with the *K*-band Keck image.

REFERENCES

Broadhurst, T., & Lehár, J. 1995, ApJ, 450, L41
Condon, J. J., Huang, Z.-P., Yin, Q. F., & Thuan, T. X. 1991, ApJ, 378, 65
Downes, D., Solomon, P. M., & Radford, S. J. E. 1995, ApJ, 453, L65
Eisenhardt, P. R., Armus, L., Hogg, D. W., Soifer, B. T., Neugebauer, G., & Werner, M. W. 1996, ApJ, 461, 72
Elston, R., McCarthy, P. J., Eisenhardt, P., Dickinson, M., Spinrad, H., Jannuzi, B. T., & Maloney, P. 1994, AJ, 107, 910
Genzel, R., Weitzel, L., Tacconi-Garman, L. E., Blietz, M., Cameron, M., Krabbe, A., Lutz, D., & Sternberg, A. 1995, ApJ, 444, 129
Graham, J. R., & Liu, M. C. 1995, ApJ, 449, L29
Iwamuro, F., Maihara, T., Tsukamoto, H., Oya, S., Hall, D. N. B., & Cowie, L. L. 1995, PASJ, 47, 265
Krabbe, A., et al. 1995, in Proc. SPIE Conf.: Infrared Imaging Systems, (Orlando: SPIE), 172
Lawrence, A., et al. 1993, MNRAS, 260, 28
Lawrence, A., Rigopoulou, D., Rowan-Robinson, M., McMahon, R. G., Broadhurst, T., & Lonsdale, C. J. 1994, MNRAS, 266, L41
Matthews, K., et al. 1994, ApJ, 420, L13
Netzer, H. 1990, in Active Galactic Nuclei, Saas-Fee Advanced Course 20 Lecture Notes, ed. T. J.-L. Courvoisier & M. Mayor (Berlin: Springer), 93
Osterbrock, D. E. 1989, Astrophysics of Gaseous Nebulae and Active Galactic Nuclei (Mill Valley: University Science Books)
Rowan-Robinson, M., et al. 1991, Nature, 351, 719
———. 1993, MNRAS, 261, 513
Scoville, N. Z., Yun, M. S., Brown, R. L., & Vanden Bout, P. A. 1995, ApJ, 449, L109
Soifer, B. T., Cohen, J. G., Armus, L., Matthews, K., Neugebauer, G., & Oke, J. B. 1995, ApJ, 443, L65
Thronson, H. A., Majewski, S., Descartes, L., & Herefeld, M. 1990, ApJ, 364, 456
van der Hulst, J. M., Terlouw, J. P., Begeman, K., Zwitzer, W., & Roelfsema, P. R. 1992, in ASP Conf. Ser. 25, Astronomical Data Analysis Software and Systems I, ed. D. M. Worrall, C. Biemesderfer, & J. Barnes (San Francisco: ASP), 131
Veilleux, S., & Osterbrock, D. E. 1987, ApJS, 63, 295
Weitzel, L. 1994, Ph.D. thesis, Ludwig-Maximilian-Universität, München
Weitzel, L., Krabbe, A., Kroker, H., Thatte, N., Tacconi-Garman, L. E., Cameron, M., & Genzel, R. 1996, A&A, in press

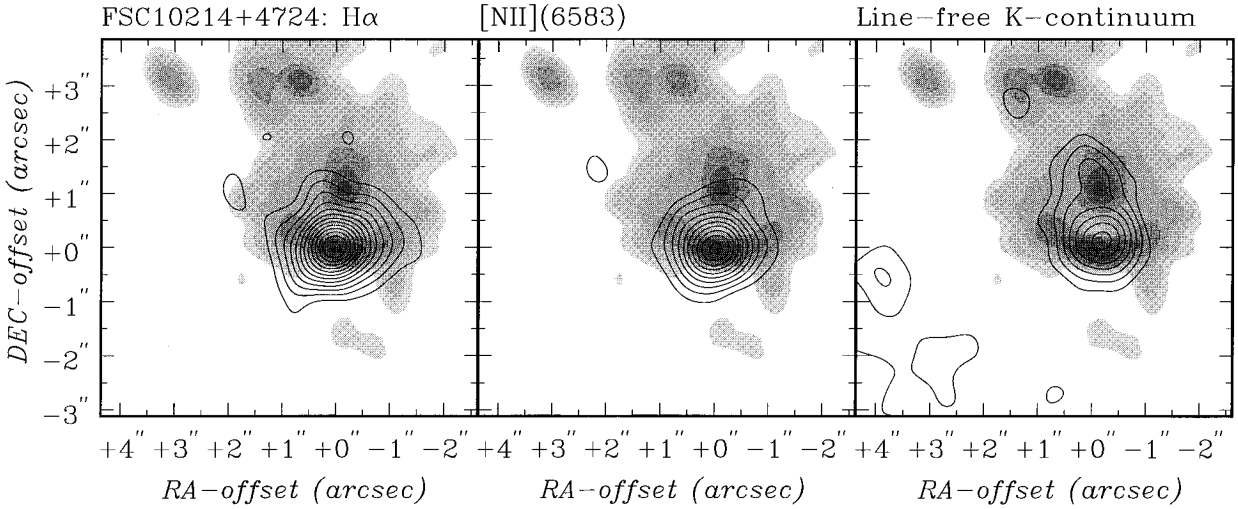

FIG. 2.—Channel maps of three spectral regions. Contours represent 3D data in linear scale, the gray scale represents the 0.″4 FWHM *K*-band maps of Graham & Liu (1995) in logarithmic scale. *Left inset*: Hα (three channels, 2.152–2.156 μm). *Middle*: [N II] λ6583 (three channels, 2.160–2.164 μm). Contours for both maps in 2 σ steps, beginning with 3 σ. *Right*: line-free *K*-continuum (98 continuum channels between 2.02 and 2.32 μm, excluding line channels). Contours are in 1 σ steps, beginning with 1 σ.